Naval Research Laboratory
Washington, DC 20375-5320

NRL/6730/MR—2023/2

Laser Machining of Sinusoidal Perturbation

MR. T. JUDE KESSLER

DR. YEFIM AGLITSKIY

DR. MAX KARASIK

DR. SASHA VELIKOVICH

Laser Plasma Branch
Plasma Physics Division

August 17, 2023

REPORT DOCUMENTATION PAGE

Form Approved
OMB No. 0704-0188

1. REPORT DATE *(DD-MM-YYYY)*	**2. REPORT TYPE**	**3. DATES COVERED** *(From - To)*
17-08-2023	NRL Memorandum Report	

4. TITLE AND SUBTITLE

Laser Machining of Sinusoidal Perturbation

5a. CONTRACT NUMBER

5b. GRANT NUMBER

5c. PROGRAM ELEMENT NUMBER

6. AUTHOR(S)

Mr. T. Jude Kessler, Dr. Yefim Aglitskiy, Dr. Max Karasik, and Dr. Sasha Velikovich

5d. PROJECT NUMBER

5e. TASK NUMBER

5f. WORK UNIT NUMBER
9387

7. PERFORMING ORGANIZATION NAME(S) AND ADDRESS(ES)

Naval Research Laboratory
4555 Overlook Avenue, SW
Washington, DC 20375-5320

8. PERFORMING ORGANIZATION REPORT NUMBER

NRL/6730/MR--2023/2

9. SPONSORING / MONITORING AGENCY NAME(S) AND ADDRESS(ES)

National Nuclear Security Administration
Department of Energy
1000 Independence Ave SW, Washington, DC 20585

10. SPONSOR / MONITOR'S ACRONYM(S)

DOE

11. SPONSOR / MONITOR'S REPORT NUMBER(S)

12. DISTRIBUTION / AVAILABILITY STATEMENT

DISTRIBUTION STATEMENT A: Approved for public release; distribution is unlimited.

13. SUPPLEMENTARY NOTES

14. ABSTRACT

This report presents a method for machining sinusoidal perturbation in polystyrene by repetitively pulsed excimer laser ablation developed at NRL. This robust method of target manufacturing can be completed in room air, without complex environmental or optical stability control, at a reasonable production rate, and is simple to adjust.

Machined polystyrene is used as experimental targets to study laser plasma interactions on the Nike Laser. Having this capability, on site, at NRL allowed for shorter iteration time for customization of the sinusoidal amplitude and wavelength concurrent with experiments. Targets with sinusoidal perturbation were used in Nike experiments range from 2 to 20 microns in amplitude and 30 to 46 microns in wavelength. Sinusoidal perturbations during production were ablated at rates of 0.07 to 0.2 microns per laser pulse.

The laser, choice of optical elements, materials, and optical configurations are described. Detailed explanations for the unique optical elements used in this method that are not part of prior Fourier ablation systems. Materials tested in addition to polystyrene and future setup recommendations are also discussed

15. SUBJECT TERMS

Laser machining	Laser ablation	Excimer laser
Sinusoidal perturbation	Fourier filter	Polystyrene ablation

16. SECURITY CLASSIFICATION OF:			**17. LIMITATION OF ABSTRACT**	**18. NUMBER OF PAGES**	**19a. NAME OF RESPONSIBLE PERSON**
					T. Jude Kessler
a. REPORT	**b. ABSTRACT**	**c. THIS PAGE**	U	22	**19b. TELEPHONE NUMBER** *(include area code)*
U	U	U			(202) 767-2222

Standard Form 298 (Rev. 8-98)
Prescribed by ANSI Std. Z39.18

This page intentionally left blank.

CONTENTS

FIGURES

EXECUTIVE SUMMARY

This report presents a method for machining sinusoidal perturbation in polystyrene by repetitively pulsed excimer laser ablation developed at NRL. This robust method of target manufacturing can be completed in room air, without complex environmental or optical stability control, at a reasonable production rate, and is simple to adjust.

Machined polystyrene is used as experimental targets to study laser plasma interactions on the Nike Laser. Having this capability, on site, at NRL allowed for shorter iteration time for customization of the sinusoidal amplitude and wavelength concurrent with experiments. Targets with sinusoidal perturbation were used in Nike experiments range from 2 to 20 microns in amplitude and 30 to 46 microns in wavelength. Sinusoidal perturbations during production were ablated at rates of 0.07 to 0.2 microns per laser pulse.

The laser, choice of optical elements, materials, and optical configurations are described. Detailed explanations for the unique optical elements used in this method that are not part of prior Fourier ablation systems. Materials tested in addition to polystyrene and future setup recommendations are also discussed

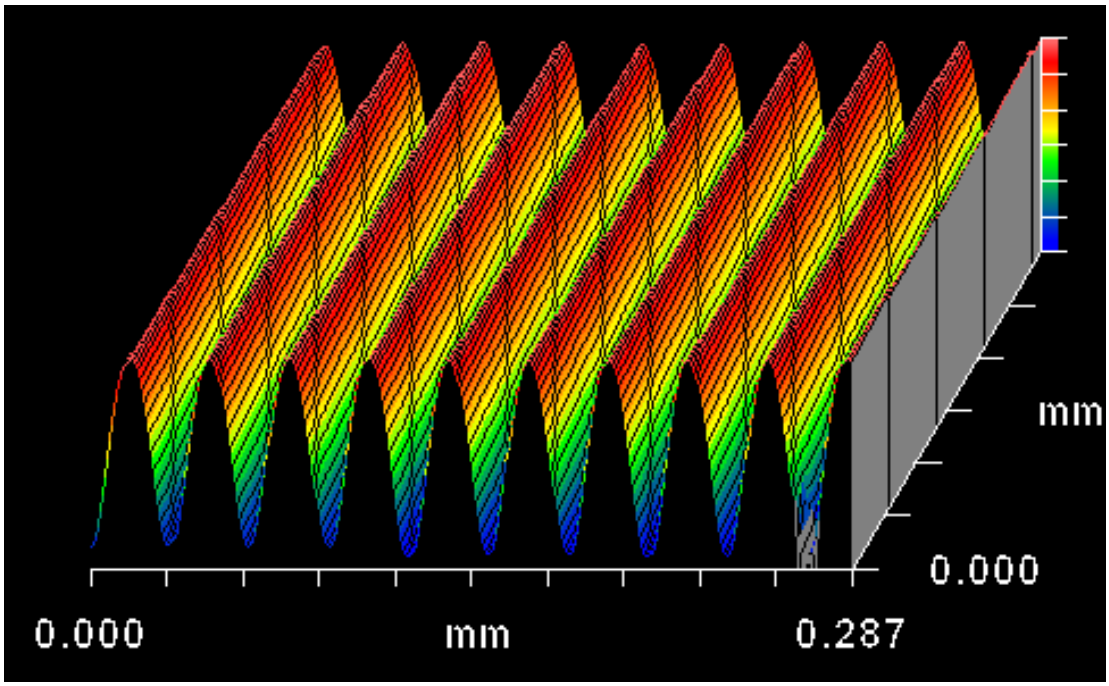

Fig. E1 — Zygo image of polystyrene target laser machined with system developed at NRL with 30nm wavelength and 2 μm amplitude sinusoidal surface perturbation.

This page intentionally left blank.

Laser Machining of Sinusoidal Perturbation

1. INTRODUCTION

Laser machining is a type of machining where a laser removes material by ablation. Commercially available laser cutters and laser engravers use a single beam moving across the surface to create a pattern through or on the surface given material. Fourier laser machining is the same laser material process, however instead of a single beam moving across a surface an imaged pattern is ablated over the area of the material surface. The desired pattern discussed in this report is a single mode sinusoid. The sinusoidal intensity pattern is formed by selecting two components in a Fourier plane [1] to form a sinusoid in the inverse Fourier plane and material surface plane. The whole process is named Fourier laser machining.

Sinusoidal perturbations on the surface of plastics are a standard type of target used in studying laser plasma interaction and instability. The sinusoidal perturbation provides a known measurable repeating pattern for seeding instability. The targets created have been used in a variety of experiments on the Nike laser [2] including Richtmyer-Meshkov instability, mass oscillation, and Richtmyer-Meshkov jet formation, and suppression of laser imprint.

Sinusoidal surface perturbations in polystyrene can be created using a variety of methods. Spin casting polystyrene [3] on machined nickel molds was the current method used for target production at the time of the development of the laser machining system. The machined turned metal molds produced a relatively large radius of curvature that approximated parallel lines over the width of the target surface. Nickel molds are effective in producing high quality experimental targets. The mold can be limited by the ability to machine a pure sinusoid rather than a step or tilted pattern. Also, any defect in the mold is transferred the casting resulting in target defects or lower yield. The material has to be cleanly lifted from the mold and then cut and assembled on to the target while maintaining a planar surface curvature. Fourier laser machining was investigated as an in-house alternative with the potential to create a sinusoidal pattern on the surface of a previously mounted flat planar polystyrene target. An additional benefit would be short turnaround time when changing wavelength or amplitude. In contrast to molds that must be machined to change either wavelength or amplitude, a change of a beamline element or number of laser pulses would change the wavelength or amplitude respectively for the next target machined.

The initial requirements for the laser machining setup were to be capable of producing a sinusoid two microns in amplitude 30 microns in wavelength, operate in a regular laboratory environment, and not require great mechanical stability. Fourier machining was chosen over two beam interference where a single laser is split and recombined at an angle to produce a sinusoidal interference pattern since the setup does not rely on stability at the interferometric level and can maintain alignment over hundreds to thousands of laser pulses.

2. MACHINIG APARATUS

The core Fourier laser machining setup is based on a design at Osaka University [4] used to ablate sinusoids with excimer laser pictured in Fig. 1. An optical system images an excimer laser backlit wire mesh onto planar polystyrene (Figures 1, 3, and 4). The wire mesh defines a two dimensional square wave pattern. A lens one focal length after the wire mesh creates a Fourier plane [1] at one focal length after the lens. At the Fourier plane the Fourier transform [5] of a two dimensional square wave is a two

Manuscript approved August 10, 2023.

dimensional array of focused spots (Grating equation d sin θ = mλ) [6]. A Fourier aperture blocks a portion of the focal spots at the Fourier plane. At one focal length after the Fourier plane second lens creates a second Fourier transform or inverse Fourier transform at the inverse Fourier plane. The Fourier filtered pattern consisting of the remaining components of the square wave pattern exists at the inverse Fourier plane. This filtered pattern is imaged onto the target surface with a third lens set at distance "a" from the inverse plane and "b" from target surface to magnify (M) the pattern on target (*Magnification: M=b/a, 1/f=1/a+1/b*).

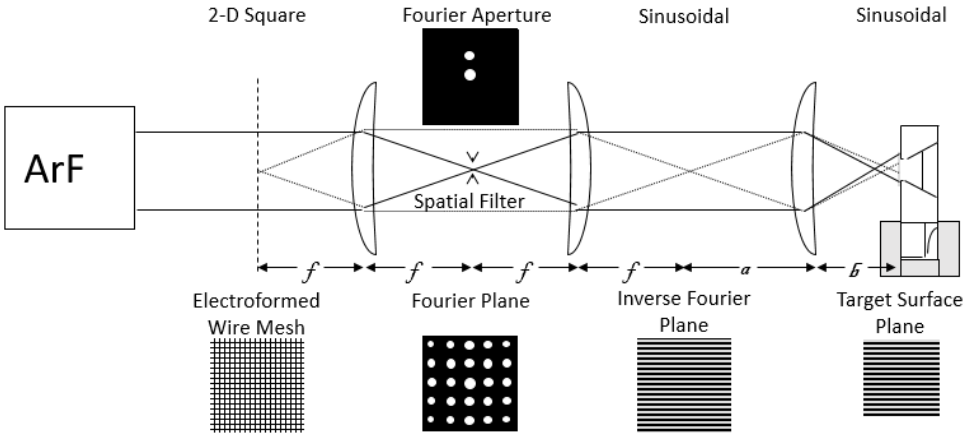

Fig. 1 — Diagram of Fourier laser machining setup similar to the setup used for machining of sinusoids at Osaka University

2.1 Previous work

Osaka University developed a laser machining system (Fig. 1) where an ArF 193 nm laser backlights the wire mesh. ArF lasers deep UV wavelength absorb close to the surface and have a low 10mJ/cm^2 laser ablation threshold for polystyrene [7]. The aperture at the Fourier plane selects two focal spots along one axis by blocking the remaining foci to filter for the first order sinusoidal wavelength. Typically the selection is the central and neighboring +1 foci along a single axis. The central foci is the brightest due to the finite illumination area. In the inverse Fourier plane the two focal spots are Fourier transformed to a sinusoidal image. This method of creating a sinusoidal intensity variation by Fourier filtering an image is stable based directly on movement of the mesh relative to the optical train and target surface rather than stability of the interference pattern. The sinusoidal intensity pattern has an intensity offset due to unequal energy between the dots.

2.2 Pattern stability

Fourier laser machining does not require the same optical component stability compared with an interferometric two beam overlap. Selecting the central zeroth and plus one vertical focal spots at the Fourier plane with will produce a sinusoid along the vertical axis and an even energy in the horizontal axis at the focal plane on the polystyrene. The Fourier transform of two dots is a sinusoid. Our understanding is that because the two beams are created by selection at the Fourier plane they maintain phase relation with small optical movements. The interference pattern is not determined by the relative position of optics changing the relative phase relationships. Movement sufficient to move the pattern between shots deleterious to the cumulative pattern would have to be on the scale feature wavelength, tens of microns. Interferometric stability is on the order of laser wavelength, nanometers.

Splitting the beam and overlapping with an angular difference would also create a sinusoidal pattern, but would have the stability of an interferometer. Consider counting a single fringe shift of a Michelson interferometer at 248nm for 30 micron wavelength intensity pattern on target. Counting one fringe is the equivalent of displacing of a 30 micron sinusoid in the intensity pattern by 30 microns at the target plane. Fringes move with changed of distance $2d=n\lambda$ where d is the change in optical path distance between the two interfered beams [8]. For a 248nm laser a 30 micron displacement, one fringe, is caused by a 124nm change in path length difference.

For the Fourier filtering method a full cycle, 30 micron displacement, requires 30 microns of optical movement along the pattern itself. The aperture selection is inherently in the same plane for the two selected beams. Optical movements along the optical train would shift the pattern as a whole rather than the interference pattern fringes making the Fourier filtering approach 250 times less sensitive. With the Fourier filtering method of selecting two beams to be interfered thermal variation, small vibrations, and air currents have little to no effect on the sinusoidal pattern or imaged position on the target surface.

2.3 NRL Setup

The Fourier laser machining setup implemented at NRL uses the same principle of imaging backlit electroformed wire mesh [9] through a Fourier filter onto the target surface Fig.3. Lenses are again spaced at one focal length distances from grating, Fourier plane, and inverse Fourier plane. The Inverse Fourier image is magnified on the target surface with a third convex lens. Two critical differences are a cylindrical lens that works with a modified Fourier aperture to select for the single mode sinusoid and an optional parallel plate translator for cumulative smoothing Fig.4. The laser is a KrF 248nm excimer laser and all optics are KrF excimer grade.

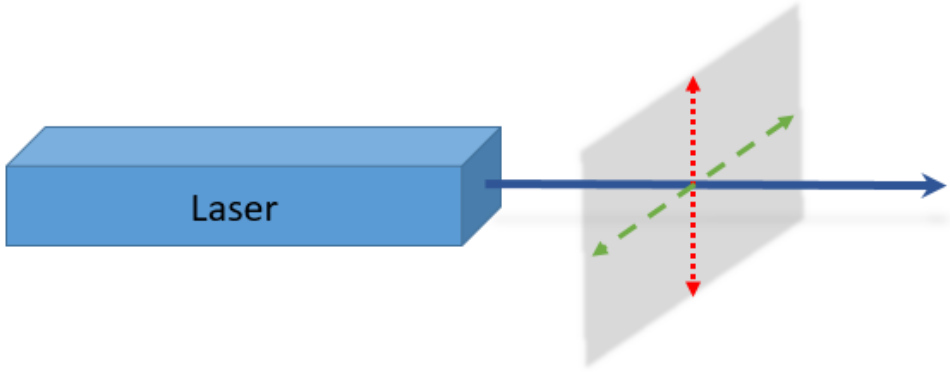

Fig. 2 — Reference axes defined
The commercial excimer lasers used or discussed have different axial divergences. For reference the axis will be labeled G-axis (green) for greater divergence and L-axis (red) and lesser divergence. In the examples shown or discussed in this report the G axis is parallel to the optical table plane or horizontal across the figure and the L-axis is perpendicular to the table or vertical.

A 248nm KrF Pulsemaster PM-882 laser was utilized. [Lumonics Pulsemaster PM-882 specifications when new: 850mJ/pulse, 12-17mmV x 29mmH, 1.5mradV, 3.5mradH, 14-26ns FWHM; As measured: 300mJ, 33ns, 16mmV x 30mmH] The PM-882 has a rectangular unpolarized output with different axial divergence [10, 11]. Difference in axial divergence is a cause for unique features in this setup. For simplicity, the coordinate system will be defined around this axial divergence such that the G-axis is the axis of greater divergence and L-axis is the axis of lesser divergence, and P for axis of laser propagation (Fig. 2).

Differences in axial divergence cause the Fourier plane focal spot plane for each axis to occur in a different propagation distances and with different focal spot sizes. Without correcting for this difference selecting a zero order and single dimension 1st order focal point in the Fourier plane become complicated

to impossible. In the setup tested the focal spot at the L-axis focal plane was elongated such that the foci overlapped along the G-axis.

The cylindrical lens combined with modifying the Fourier aperture is a novel way to overcome the axial divergence disparity. The modified Fourier aperture is a slit allow in two lines of foci though and only filtering the L-axis. A one dimensional sinusoidal pattern is selected for at the Fourier aperture taking the zeroth and first order foci dimension along the L-axis. All foci along the G-axis are allowed to pass though leaving a square wave pattern at the inverse Fourier plane along the G-axis. Selecting the zero and 1st order along L-axis while leaving the G-axis unfiltered at the Fourier aperture does not require both dimension to come to a focus in the same plane. The cylindrical lens moves the G-axis image plane sufficiently away such that no pattern is ablated along that dimension.

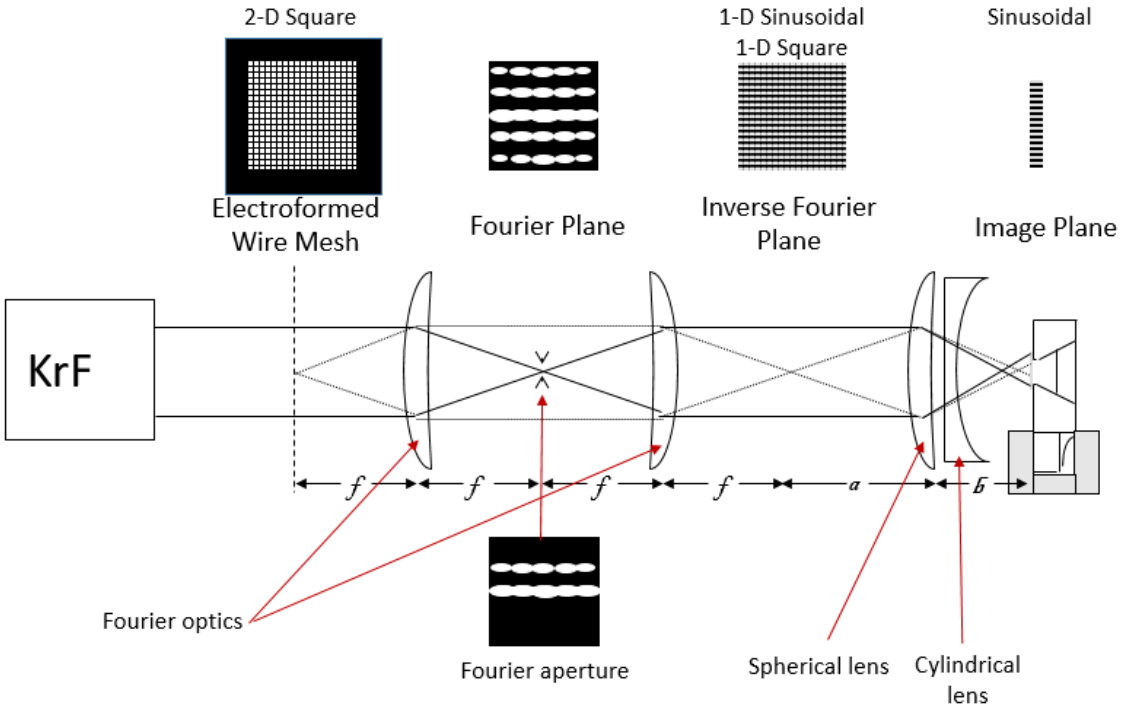

Fig. 3 — Diagram of NRL developed Fourier laser machining setup with cylindrical lens and modified Fourier aperture. *Cylindrical lens shown in top down view instead of side view to display curvature. Actual curvature is aligned along the G-axis.

2.4 Cylindrical lens

The cylindrical lens, shown in Fig.3 located between the magnification lens and target plane, changes the pattern on target from a sinusoidal L-axis and square wave G-axis at the inverse Fourier plane to a sinusoidal L-axis and flat G-axis at the Image plane. The cylindrical lens is aligned along the G-axis and the curvature effects only the focal geometry along the G-axis such that he beam does not propagate though focus between the magnification lens and the target plane. This change in imaging is an additional variable in setting intensity and also the image or perturbation intensity on target. The slit Fourier filter selects for a sinusoid along the L-axis and all modes along the G-axis leaving the square wave restored at the inverse Fourier and target planes. The cylindrical lens moves the imaged square wave pattern plane sufficiently far away from the target surface plane such that intensity perturbation is minimized on the target surface.

Cylindrical lens position does not have infinite position possibilities. Due to Talbot self-imaging [12] only planes in the phase perturbation part of the Talbot cycle [13] are without intensity pattern at the center area of the beam. A structured pattern self-images by Talbot cycles in space as it propagates. This repeating pattern of self-imaging occurs in Talbot lengths. The cylindrical lens changes the magnification of the self-imaging pattern and what fractional part of the Talbot phase-intensity cycle is on target. The cylindrical lens must be positioned at a plane where modulation is in phase and not intensity that also coincides with the desired irradiance on target surface. At such a plane the central area will have phase modulation and flat intensity while the edges will have intensity and phase modulation.

Consider a single sinusoidal pattern will alternate between intensity to phase structure in a repeating manor according to Talbot imaging cycle. Planes where major pattern components align to phase rather than intensity modulation at ½ Talbot cycles. Given the square wave input or summation of sinusoids there are many additional non-focal planes where phase structure exists. When a plane wave is incident on the wire mesh the grating pattern and higher orders will be repeated in space. So the Cylindrical lens must be positioned to avoid Talbot image planes and prominent fractional Talbot planes that line up with other major square wave components. The mesh used in this experiment is greater than 50% open space where light transmits though. The mesh should not be considered as an array of point emitters. As such there are many planes that do not line up with prominent Talbot lengths and fractional Talbot length. Smaller fractional lengths are effectively blurred out to approximate a flat wave pattern.

2.5 Parallel plate scanner

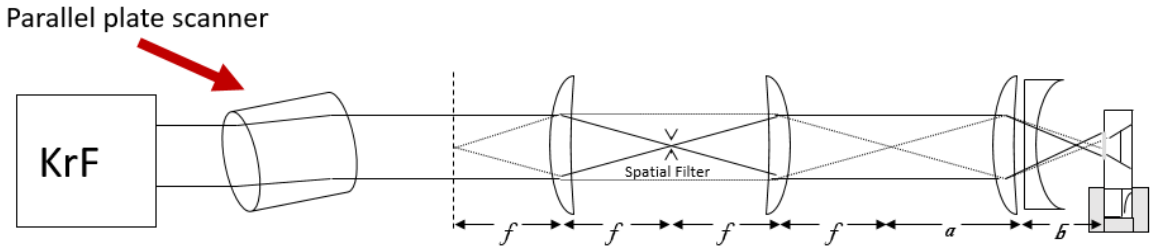

Fig. 4 — Fourier laser machining setup with beam smoothing parallel plate scanner

An optional fused silica cylindrical parallel plate scanner [14] is used to smooth laser beam uniformity variation over cumulative laser ablation pulses. Non-uniformity in the beam, such as hot spots, produce uneven ablation of the target surface. To reduce the effect of beam non-uniformity a parallel plate fused silica cylinder is inserted before the wire mesh (Fig.4). Rotating the parallel plate between laser pulses translates the beam across the backlit wire mesh in the L-G plane without changing the propagation axis angle. Translating the beam with a parallel plate rather than a turning mirror preserves the beam orientation, sinusoidal alignment on target, and location of foci at the Fourier plane, but does correspond to translation of the beam related intensity variation of the image at the target surface. Intensity variations in the laser beam are smoothed over the cumulative ablation of the surface.

However, there are requirements to beam smoothing. This smoothing approach only works if all intensity of the ablated region are within a linear part of the ablation curve (Fig. 6). The edge of the beam has intensity variation and is outside the region of linear ablation. Any non-linear region will result in non-sinusoidal ablation. So the translated beam cannot over-scan or even be scanned fully across the surface of the ablated surface. The usable region is reduced in area by the percentage scanned [Usable area = Usable Imaged pattern*(1-scan %)]. Using the scanning cylinder is a good option for reduction of small scale beam irregularity, but does little to reduce intensity gradient across the whole beam.

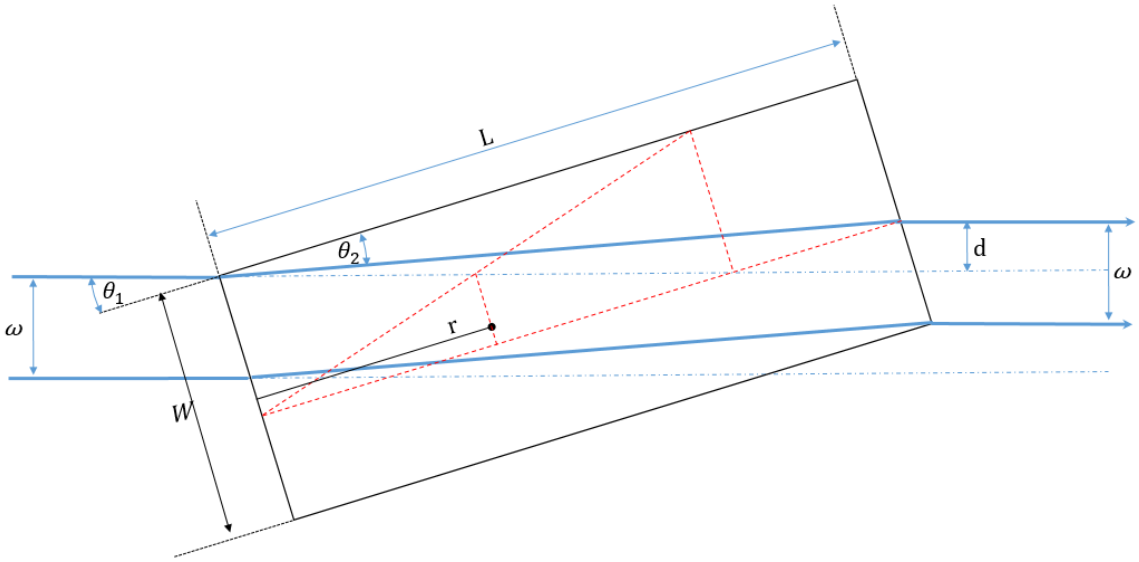

Fig. 5 — Two dimensional drawing of parallel plate scanner. Blue beam of width w refracts at maximum angle θ_1 ≤10° through the fused silica cylinder of clear aperture width W and length L to translate beam by displacement d. Red lines show use of parallel plate for a single ray and illustrate how rotation position at distance r from cylinder input surface is found.

The fused silica cylinder is a custom optic. When using the smallest necessary dimensions to achieve desired translation he optimized point of rotation point (r) is located between the input surface and the midpoint of the parallel plate (Fig.5). Here are some useful equations for determining minimum cylinder Length (L), minimum cylinder clear aperture width/radius (W) and rotation point (r) for a desired translation distance (2d), beam width (ω), maximum input angle(θ_1) ≤ 10°, index of refraction air (N_1), and index of refraction cylinder (N_2). Position r is a point along the center axis of input and output planes and is located towards the input surface rather than the midpoint except for the single ray limit where ω=0. Note, for a given translation distance Increasing parallel plate width for clear aperture buffer and length to decrease θ_1 can be considered with respect to the increased of cost of larger excimer grade material that maintains homogeneity, parallelism, and surface quality.

$$W = L * tan\left(sin^{-1}\left(\frac{sin\,\theta_1 * N_1}{N_2}\right)\right) + \frac{\omega}{cos\,\theta_1} \qquad L = \frac{d/cos\theta_1}{tan\theta_1 - \tan\left(sin^{-1}\left(\frac{Sin\theta_1 * N_1}{N_2}\right)\right)} \qquad r = \frac{W - \frac{\omega}{cos\,\theta_1}}{2\,tan\,\theta_1}$$

For a proof of concept an existing 60mm long 40mm in diameter fused silica cylinder was utilized. The 40mm diameter is sufficient for the beam size given the 60mm length. The 60mm length sets the maximum beam displacement to 3.4mm for a 10 degree rotation.

2.6 Ablation rate

In order for a sinusoidal intensity pattern to ablate a sinusoidal surface perturbation the entire range of fluence must be within a linear region of the ablation curve and above the ablation threshold. The ablation curves (Fig. 6) plot single laser pulse ablation depth as function of fluence with 33ns FWHM in air and vacuum and 55ns in vacuum. Material was ablated using the same laser and polystyrene film used for sinusoidal patterned ablation. Ablation depth was measured by Zygo microscope. Establishing a laser and diagnostic specific ablation curve is useful for determining the working range of usable fluence. The shape of the measured ablation curve is in line with other known Polystyrene ablation curve for 248nm laser [15].

Over this fluence range laser ablation has two primary mechanisms of photo-chemical and photo-thermal [16]. Photo-chemical is the direct breaking of bonds due to photon absorption. Photo-thermal is the result of increased temperature from photon absorption. The rapid rise in ablation depth around 400mJ/cm2 is where the ablation mechanism transitions from photochemical to photo thermal dominant. At fluence below this transition as the fluence increases above the ablation threshold of the ablation depth increases mostly linearly as a function of fluence and is photo-chemical ablation. The ablated material does attenuate fluence at the surface. In the photo-thermal region of the curve the attenuation becomes a larger factor resulting in the slower rise above ~600mJ/cm2

For a single laser pulse ablation occurs in the three phase of preablation, ablation, and post ablation as explained by Sylvain Lazare and Vincent Granier [17]. In preablation, before ablation starts, light absorbs into the volume of the polymer according to a Lambert-Beer law $I(x,t) = I_0(t)e^{-\alpha(t)x}$ where $I_0(t)$ is the unobstructed light intensity, $\alpha(t)$ is the dynamic absorption coefficient, and x is the depth below the surface. During the ablation phase intensity is above the ablation threshold. Ablated material screens the underlying solid surface such that intensity reaching the surface is $I_s(x,t) = I_0(t)e^{-\beta(t)x(t)}$ where $\beta(t)$the dynamic absorption coefficient is and $x(t)$ is the position of the solid-vapor interface with respect the initial surface. When intensity reaching the surface is no longer above threshold the pulse enters post ablation and energy reaching the surface absorbs into the volume as it did in preablation.

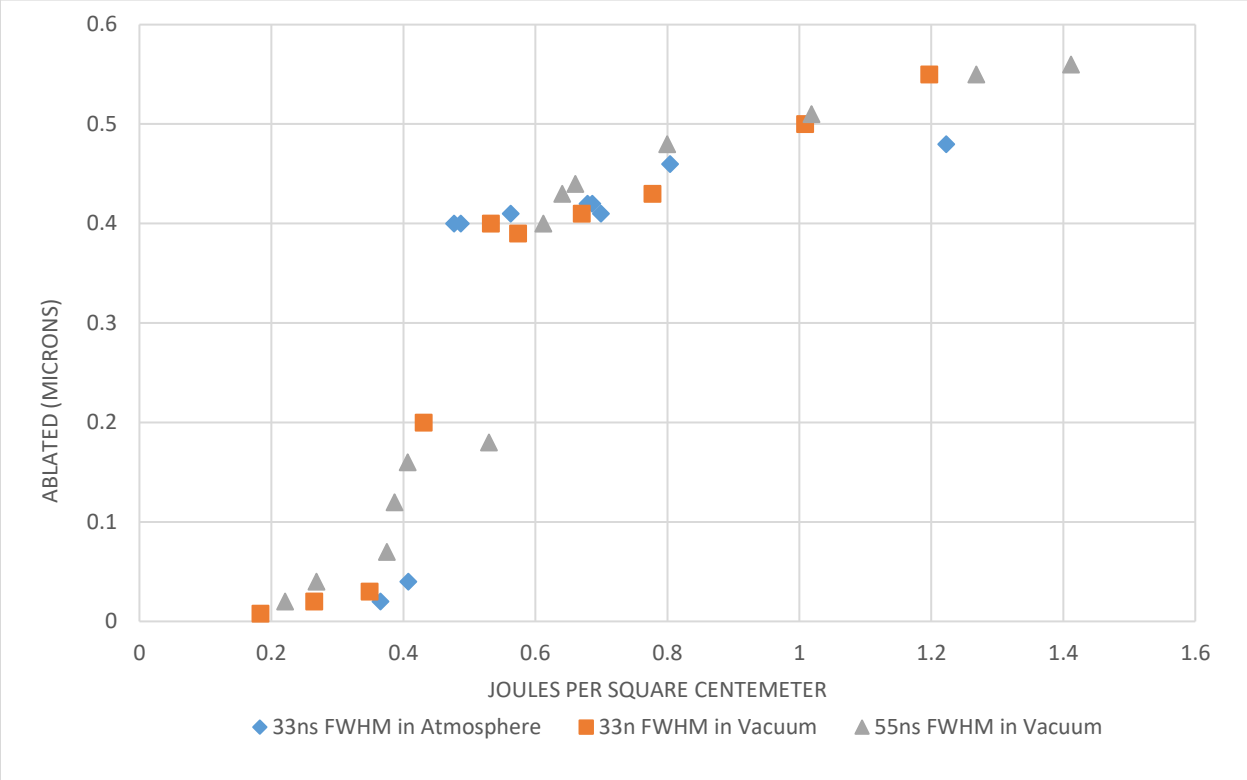

Fig. 6 — Ablation depth in polystyrene as a function of KrF 248nm fluence. Depth measured by Zygo white-light interferometric microscope. Pulse length FWHM of 33ns and 55ns in vacuum and 33ns in air shown.

The ablation curve has regions of relatively linear ablation rates. The ablation threshold for polystyrene at 248 nm is 57mJ/cm2 in vacuum and 33mJ/cm2 in air [7]. Staying in the photo-chemical range [18] is the most flexible region for patterned ablation as the sinusoidal contrast requirements are less constrained. Also, at a lower rate of ablation the beam fluence is attenuation by less ablated material and is less detrimental to ablation depth approximating linear dependence on fluence.

The energy difference between the central order and 1st order gating maxima is preferential to two maxima of equal intensity. The difference in focal spot energy creates an offset sinusoidal intensity pattern that is always above the ablation threshold. A pure sinusoidal perturbation in the laser intensity would not translate to a sinusoidal laser machined surface. Any part of the intensity pattern below threshold would not ablate any material resulting in flat topped peaks in the surface. The entire intensity pattern must have single pulse fluence in the linear ablation range in order for a sinusoidal intensity pattern to produce a sinusoidal ablation pattern.

3. EXPERIMENTAL TARGET PRODUCTION

The intended use of the laser machined sinusoids is as targets in Nike Laser experiments. Laser machined targets have been use for alignment and calibration, part of an experimental set, and primary target type across several experiments. Three setups discussed below cover the range of laser machined targets produced for published Nike experiments.

3.1 What is a successful target?

Ideally all sinusoidal targets would be pure single mode sinusoids. However this is not the case whether the targets are Laser machined, cast, or mechanically machined. The degree to which a target must be sinusoidal is dependent on the constraints of the experiment and method of measurement. At minimum, a target must be a near sinusoid having continuous repeating pattern where a single peak and trough per cycle separated by a consistent known wavelength and amplitude. A good sinusoidal profile when measured with Zygo white light interferometer would have a ratio of primary sinusoidal mode to higher order mode of at least 10:1(see Fig.9). For amplitudes significantly higher than 2 microns the amplitude is determined by interferometer and profile by side view x-ray or digital camera (Fig.10 and Fig.11).

3.2 Production method

Each target is laser machined on a substrate previously mounted on a Nike target mount. Polystyrene substrates used originated from preassembled flat polystyrene produced and mounted by Schaffer Corporation or from rolls of Goodfellow polystyrene cut to specified width and glued onto Nike style mounts.

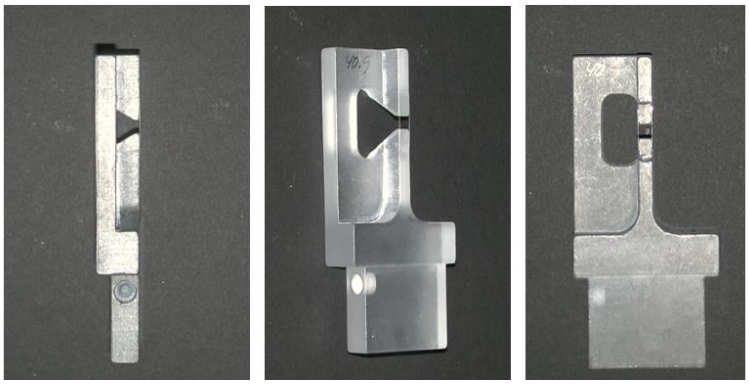

Fig. 7 — Side (left), angle (center), and front (right) view of standard Nike mount with 3mm wide polystyrene target mounted across the jaws.

After mounting, each target was exposed to low level uniform KrF laser light. A relatively low intensity uniform source is created by placing a diffuser in the path of the laser beam. The purpose of pre-exposing the material is to clean and prepare it for ablation. Intensity is restricted to near the ablation threshold such that the rate of ablation is low or none. A relatively few exposer pulses in uniform laser light does not contribute to the ablated profile and is not a measurable change to the target surface profile under examination with Zygo interferometer. This exposer removes dust and debris on the surface. It also exposes the target volume to laser light. If there is a cumulative effect to the ablation threshold then this will lessen the effective difference between sinusoidal intensity with respect to the ablation threshold [7]. The illumination aperture around the mesh is a rectangle of (1.2cm L x 2.1cm G) but is not required to be an exact rectangle. In order for pattern intensity to be uniform the total energy illumination across the mesh has to be equal. A custom shape aperture can be cleverly used to compensate for poor beam uniformity gradients. There are some situations where a non-rectangular aperture will produce a more uniform pattern over the desired ablation area at the target plan than a rectangular aperture.
Nominal lens focal length is f=200 mm for round convex lenses and f=150mm for concave cylindrical lens. Magnification of the image sets wavelength feature size on the target surface as well as fluence proportional to the change in area. Due to physical limitation for a given aperture slit with a given optical setup there are a range of viable mesh sizes that allow for selection at the Fourier aperture. Mesh is listed in lines per inch. Too many lines per inch causes the foci to separate beyond the available aperture adjustability. Practically beyond the 2 inch sized optics used on the beam path. Too few lines per inch and the lines become hard to separate at the aperture. For the experimental setup used 400-500 lines per inch provided the best results compared to the next available 333lpi (lines per inch) and 750lpi meshes. This restriction is due the particular laser and optics and Fourier aperture slit range of opening.
For example (see Fig. 3), to produce a 30 micron wavelength sinusoidal perturbation a 500 line per inch wire mesh is selected. A 500 line per inch mesh equates to 50.8 micron line separation and 50.8 micron wavelength sinusoid at the inverse Fourier plane. To obtain the desired 30 micron wavelength the Magnification lens is positioned based on thin lens equation such that:

$$\text{Magnification} = \frac{\text{distance targert plane to magnification lens}}{\text{discance inverse Fourier plane to magnification lens}} = \frac{\text{desired pertibation wavelength}}{\text{Wavelength at inverse Fourier plane}} = \frac{30\text{ microns}}{50.8\text{ microns}}$$

To select the two lines of foci at the Fourier plane the Fourier aperture slit width is set based on the focal spot separation. Focal separation is determined using the grating equation: $d\sin\theta = m\lambda$ where $\sin\theta = \lambda/d$ for m=1. The Fourier plane is one lens focal length, 20cm, away from the first Fourier lens. So the aperture separation is twice the foci separation at the Fourier plane in order to select two foci.

$$\text{Aperture slit seperation} = 2 \times \text{lens focal length} \times \sin\theta = 2 \times 200\text{mm} \times \frac{248\text{nm}}{50.8\mu\text{m}} = 1.95\text{mm}$$

Each target to be laser machined is placed in a target holder that is aligned to the front side so that each target is in the same plane as the previous. The ablative process takes place over multiple pulses. Pulse rate 1-1.5 Hz for 0.5 to 30 minutes depending on rate of ablation and desired perturbation amplitude. Ablation depth per pulse nominally 0.01 microns per pulse over the cumulative pulses for each machined target.

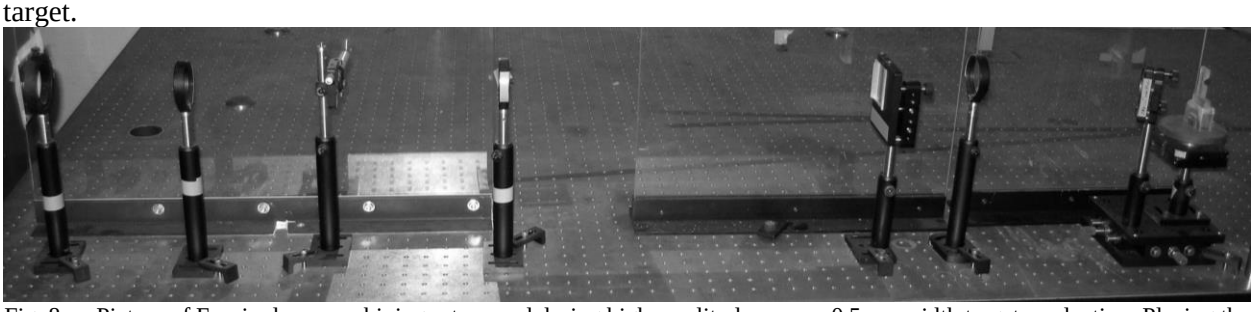

Fig. 8 — Picture of Fourier laser machining setup used during high amplitude narrow 0.5mm width target production. Placing the cylindrical lens before the magnification lens was found to be the optimal location for pattern and intensity uniformity over the target surface area

3.3 2 micron amplitude 30 micron wavelength

The initial goal was creating two micron amplitude thirty micron wavelength perturbation using the full system including parallel plate beam smoothing as a direct comparison to mold produced targets with the same wavelength and amplitude. To produce 30 micron wavelength a 500 line per inch mesh produces sinusoids with 50.8micon wavelength in the inverse Fourier plane. Magnification=30/50.8=0.59. Over tens to hundreds of shots the cylinder as manually scanned in a pattern of pitch and yaw adjustments up to +/- 8 degrees combined. Targets were successfully machined with highly sinusoidal single mode perturbations of 30 micron wavelength around two micron amplitude (Fig.9). Several proof of concepts targets were created and the highest quality targets that matched wavelength, amplitude, and single mode contrast ratio were tested against mold cast targets made by Schaffer Corporation and produced similar experimental results to those in an experiment studying laser imprint with uncoated and metal coated polystyrene targets with sinusoidal perturbation [19].

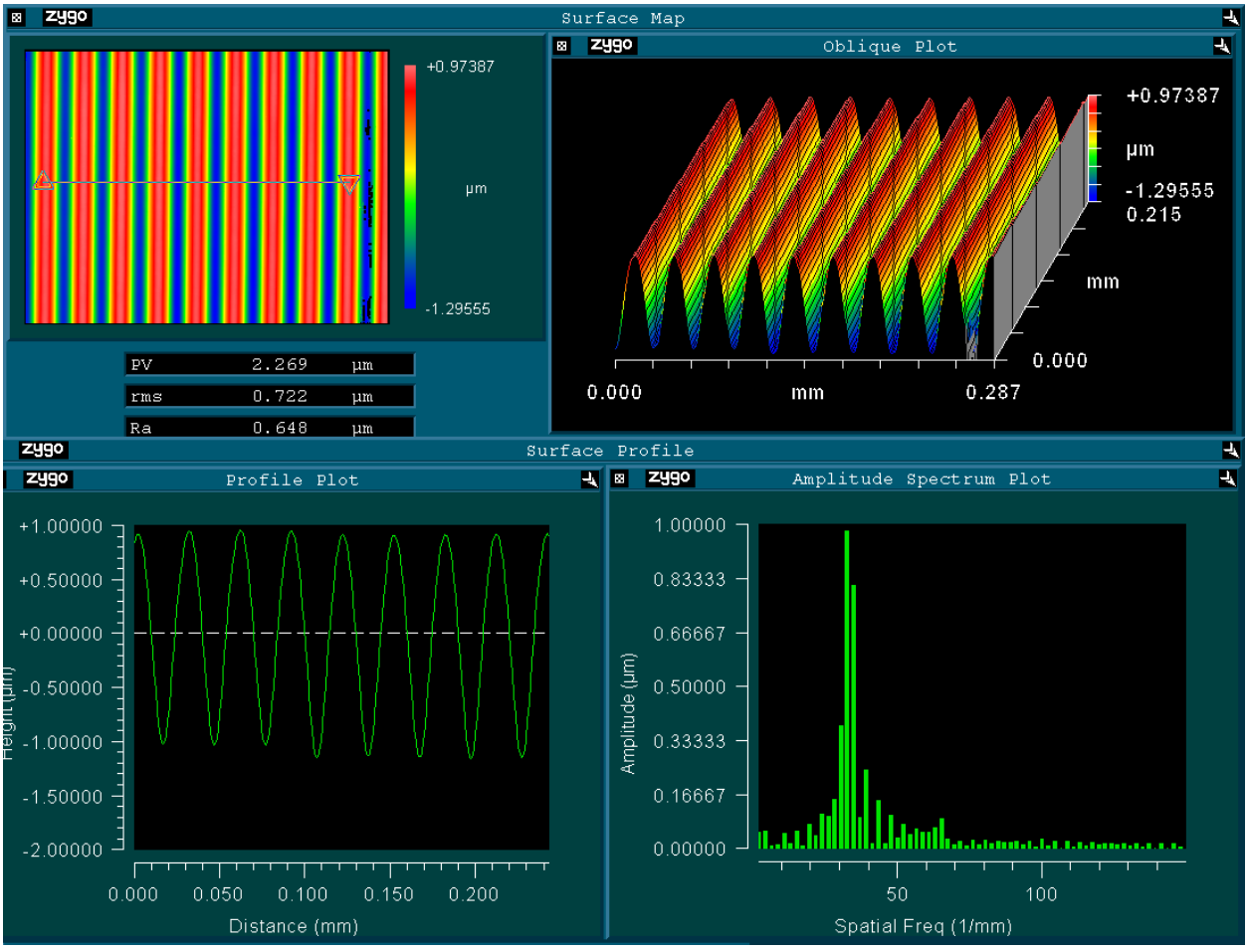

Fig. 9 — Fourier laser machined target surface measured with Zygo New View 5000 scanning white light microscope. Profile plot (bottom left) of line in top left surface image displays 2 micron peak to valley amplitude. Amplitude spectrum plot (bottom right) indicates dominant single mode spatial frequency with greater than 10:1 contrast compared to second order spatial frequency for 30 micron wavelength target.

3.4 5 micron amplitude 30 and 45 micron wavelengths

Targets 30 and 45 micron wavelengths with 3 to 8 micron perturbation amplitude, 500 microns wide, and substrate thicknesses from 53 to 125 microns were created for an experiment studying the evolution of unsupported shock with a seeded hydrodynamic perturbation [20]. In the experiment a 350-450ps laser pulse irradiates the front rippled target surface. The sinusoidal front surface perturbation seeds initial areal mass modulation growth. After the laser pulse the areal mass modulation is observed undergoing multiple phase reversals.

To produce 30 micron wavelength a 500 line per inch mesh produces sinusoids with 50.8micon wavelength in the Fourier plane. Magnification=30/50.8=0.59. For 45μm a 400 line per inch mesh was used. Magnification lens and target plan were adjusted such that. Magnification= 45/63.5=0.71. After each adjustments in magnification lens position the Cylindrical lens was adjusted to find best intensity and uniformity using camera at target plane equivalent positon. Talbot cycle length and major fractional Talbot cycle length planes had to be avoided.

Beam smoothing was not used during this machining run. The desired target width was only 500 microns wide. The narrow target width was positioned over the most uniform section of the sinusoidal pattern reducing the additional benefit from aggregate beam smoothing.

Targets exceeding 2μm in amplitude could not be fully measured with the Zygo white light interferometric microscope alone. The peaks and valleys were measurable features, however the rise and fall were not captured due to an insufficient amount reflected light. The perturbation amplitude was determined with the interferometric microscope, but the shape was measured with side view camera and x-ray backlit radiographic images.

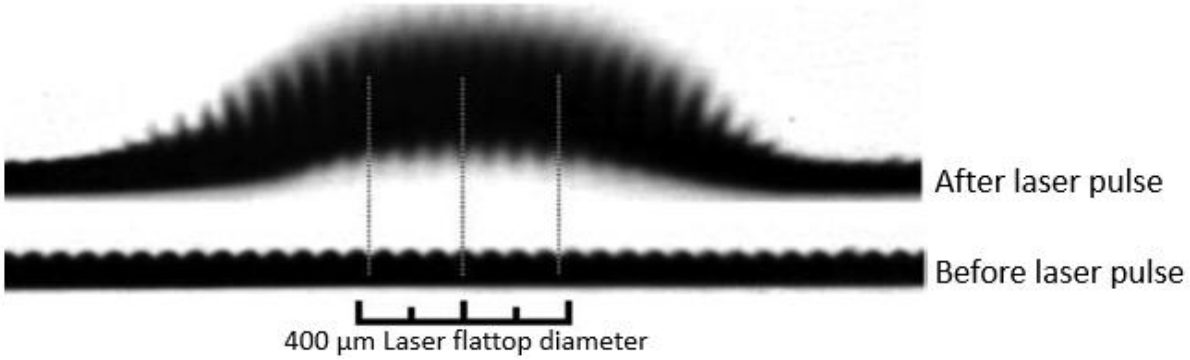

Fig.10 — Example of x-ray image of laser machined target with nominal sinusoidal amplitude of 15μm and 46μm wavelength used in Richtmyer-Meshkov jet formation experiment [11] on the Nike laser. X-ray image of target before laser pulse (bottom). X-ray image of the same target 16.5 ns after laser pulse (top).

3.5 15 micron amplitude 46 micron wavelength

Targets produced for Aglitskiy et al [21] required ripples on the rear surface of the target. The targets flat front surface was driven by a 4ns laser pulse creating a plane shock wave that propagated until reaching the rear sinusoidal surface. The shock breaking out from the rear surface was recorded by x-ray backlit imaging. Formation of jets developing aligned with the sinusoidal valley, rear interface closest to the front surface, were observed (Fig.10).

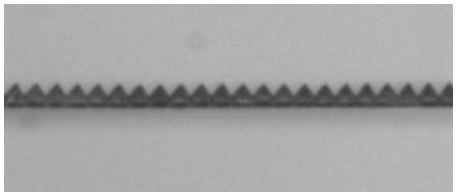

Fig. 11 — Example of a target with an amplitude too large to measure even, to find the peak and trough separation, with the Zygo interferometer. Side view picture of 46 micron wavelength target shows high amplitude in access of 20 microns. Target not characterized further due to amplitude exceeding experimental requirements.

To create these targets a 500 µm wide 53 µm thick polystyrene strips were mounted to the front of the Nike target mounts. The Nike targets mounts only attach the target material on the top and bottom. The target has open access from the sides of the as well as the rear. The target mount was rotated 180 degrees in the holder such that rear target surface faced laser. The p-axis position of target holder was adjusted to align the rear surface with the ablative target surface plane. Sinusoidal single-mode ripple wavelengths of λ=46µm and nominal peak-to-valley amplitude of 15µm were laser machined directly on the rear surface of the target. The amplitudes produced far exceeded the range to be fully characterized by the Zygo white light interferometer. For perturbation amplitudes around the 15µm experimental range amplitude height was determined by taking the difference between observing fringes with the Zygo white light interferometer at the peak and valley while varying objective height above target. Also, side view profile was taken during the experiment to measure target alignment and perturbation shape Fig.10. Some targets greatly exceeded the experimental requirements having perturbations over 20µm in amplitude. Measuring the difference between peak and valley fringes with the white light interferometer was no longer viable and amplitude was estimated based on side view images Fig.11. Such targets were still useful for diagnostic alignment purposes.

Sinusoidal Wavelength	Targets Machined	Amplitude range µm	Modal Amplitude µm	Nominal Thicknesses µm
30	87	1.7-9.3	5	53, 100, 125
45	27	2.8-9.7	5	125
46	66	5.4-23+	15	53

Fig. 12 — Table of machined targets describes in 3.4 and. 3.5. Targets are grouped by Sinusoidal wavelength with listed values for number of targets machined, range of sinusoidal amplitude, most common amplitude, and polystyrene substrate thickness. Targets machined concurrent with experiments determined modal amplitude based on experimental needs.

4. OTHER MATERIALS TESTED

The primary material tested was polystyrene. However, carbon resorcinol-formaldehyde (CRF) foam [22] and polypropylene were also considered for creating experimental targets with sinusoidal perturbation by excimer Fourier laser machining. Two classes of experimental targets used in plasma instability experiments are solid plastic and foam. Polypropylene was investigated as a potential alternate solid plastic to polystyrene. Compared to solid polystyrene, solid polypropylene targets could be constructed on the micron scale opposed to tens of microns because polypropylene is both more elastic and less brittle. Many experimental foam targets, such as resorcinol-formaldehyde (RF) must be stored in a dark inert gas. In contrast, CRF foam was a candidate for laser machining because it could possibly survive prolonged exposer to room air environment, repetitive ultraviolet laser pulses, and shock from the ablative machining process. Material samples were provided by Eric Harding at the University of Michigan for testing laser ablation as a process for patterned ablation. If successful targets were to be used similar to the patterned CRF targets used in an experiment using high energy density plasma driven by laser pulse to crease supersonic shear[23].

CRF was directly tested against polystyrene using the existing setup. CRF foam was not measureable with Zygo microscope. Due to the high absorption of visible light the surface was not detectable by white-light interferometer either before or after ablation. Side view imaging with rear lighting did show a pattern, but presented similar difficulties in determining precise alignment due to light absorption and target width. So the character of the sinusoid and amplitude could not be measured precisely with standard techniques to establish a linear ablation range. However, initial results did indicate that it would be a potential material for sinusoidal ablation with the given setup. Laser machined targets were measured by scanning electron microscope at University of Michigan and showed promising results (Fig.13). Despite not being perfect sinusoids the images show that pattern ablation occurred. With additional testing finding an appropriate intensity region with minimal changes to the setup used for machining polystyrene is plausible.

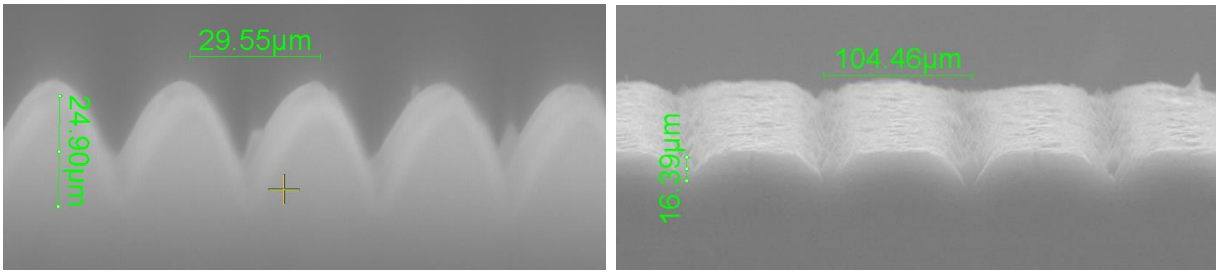

Fig. 13— Sample images of laser machined CRF foam targets. Measurements made with scanning electron microscope at University of Michigan.

Polypropylene was not successfully ablated in any of the attempts. No sign of machined perturbation was detected by white light interferometry, microscope, camera, or by diffraction. The probable reason for this is that the fluence was below ablation threshold [24]. Transmission of 248nm light through polypropylene was measured by spectrophotometer. Polypropylene is mostly transparent at 248nm. In contrast, Polystyrene is a highly absorbed at 248nm. Show in Fig.14 is a transmission curve for 8 µm and 75 µm thick Polypropylene. At 248nm 75 µm polypropylene transmits the majority of the light indicating that much less is being absorbed on or near the surface compared with polystyrene where 53 µm. Without sufficient fluence to reach higher absorption polypropylene is not a good candidate for target manufacturing at 248nm using the fluence range provided with the current setup. To even achieve 50% attenuation from absorption 425 micron thick polypropylene is required based on Beer's law $\ln\left(\frac{100}{\%T}\right) = \mu d$ where %T is the transmission percentage at depth (d) and μ is the attenuation coefficient. Beer's Law is satisfied for both 8 micron and 75 micron thick polypropylene if cumulative Fresnel surface reflection is 12.3% and $\mu = 0.00163$
(Corresponding index of refraction is calculated to be 1.65 @248nm).

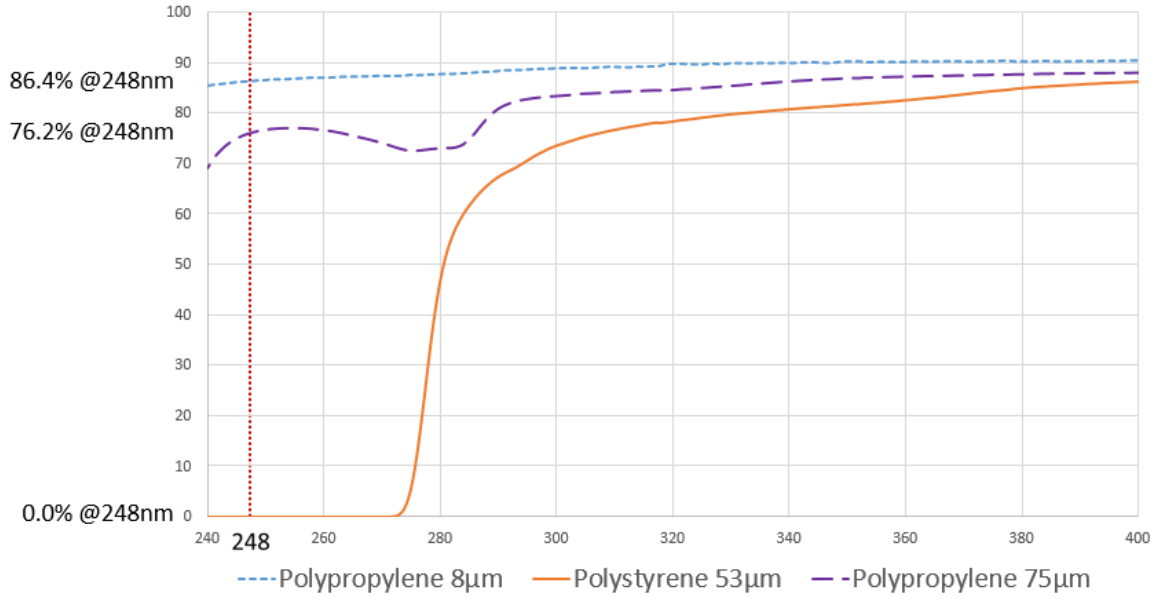

Fig. 14 — Spectrophotometer Transmission measurement of 53 micron Polystyrene (Orange) and 8 and 75 micron Polypropylene (blue and purple respectively).

5. CONCLUSIONS, NEXT STEPS, AND FUTURE IMPROVEMENTS

Experimental targets were produced successfully in polystyrene over a range of perturbation wavelengths and amplitudes using Fourier laser machining with KrF laser. Based on the testing and successful production of targets several improvements to the system could be made. Improvements would allow greater range of ablated wavelengths, ablated materials, area of ablation, and purity of single mode sinusoidal perturbation.

Changing the type of excimer laser from KrF at 248nm to ArF at 193nm could benefit from the lower wavelength. Lower wavelength 193 nm light absorbs closer to the surface compared to 248nm light resulting in a lower 10mJ ablation threshold [7]. The lower threshold and lower transmission depth could provide a cleaner ablation with less thermal energy going into material that is not ablated. The lower wavelength is absorbed a larger variety of material making it a potentially better choice for ablation of other material such as polypropylene and foam [25]. At minimum, to closely replicate the same setup for use with an ArF laser excimer grade uncoated or 193nm anti-reflective coated optics would be required. To use the same mesh and aperture the Fourier lenses focal length would have to increase by 248/193 to maintain the same foci separation at the Fourier plane due to the change in wavelength.

Selecting a laser or oscillator-amplifier laser pair with lower divergence, uniform divergence, and larger uniform beam area would reduce focal spot size at the Fourier aperture. Smaller focal spot size would allow for greater flexibility in Fourier aperture and allow for a larger range of wire meshes and aperture types. The range of wire meshes that produce a Fourier aperture selectable sinusoid correspond to the range of possible sinusoidal wavelengths. Under certain conditions the Fourier aperture selection of two focal spots to create sinusoidal perturbation would be possible with the associated intensity loss on target.

When integrating parallel plate into the setup the highest quality sinusoids were produced in terms of uniformity and purity of sign wave. Within the measurement limit of the white light interferometer the sinusoidal perturbations meet or exceeded the best examples of sinusoids made with molds with a 15-1 first to second order sinusoidal signal ratio. The limitation of this technique is that ablation does not fall off linearly and while the center of the target was an ideal sinusoid the edges were not. Translating the beam around therefore reduces the area of the usable center. A larger more and powerful laser beam with a larger parallel plate sufficient to make the beam size much larger than the target would increase the central overlapping ablation area to match the target area.

Additional lens options with longer focal length lenses used to create the Fourier and inverse Fourier planes would also allow for a larger verity of wire mesh lines per inch to be used. Longer focal length lenses would increase separation of the focal spots at the Fourier plane to set the wavelength at the inverse Fourier plane and target perturbation wavelength. The wavelength can be changed by altering the magnification from the inverse Fourier plane to the target plane. However, that also changes the image area and fluence. This is most useful for producing longer wavelength perturbations from lower lines per inch meshes where the foci separation at the Fourier plane would otherwise be smaller.

An alternate pattern seed worth testing is replacing the mesh with a sinusoidal perturbation in either transmission or surface perturbation. A sinusoidal or near sinusoidal diffraction grating would be an efficient seed. Ideally this setup would only require imaging. However, gratings are not typically perfect and cleaning up additional modes with a Fourier aperture would still be necessary to select a single mode sinusoid. The amount of energy lost to these modes would be significantly less than when starting with a square wave. Also, the required diffraction grating would still need an intensity offset so that intensity does not fall to zero. An ideal grating would have a Fourier transform consisting of two foci where one has a much greater intensity relative to the other.

The recommended changes prescribe what could be done to improve the range and usability of the setup. The results documented in this report were a highly successful demonstration of functional concept using existing lasers, diagnostics, a few new lenses, and inexpensive wire meshes.

REFERENCES

1. Hecht, Eugene, and Alfred Zając. 1974. “Optics,” Addison Wesley Publishing Company.

2. S. P. Obenschain, S. E. Bodner, D. Colombant, K. Gerber, R. H. Lehmberg, E. A. McLean, A. N. Mostovych, M. S. Pronko, C. J. Pawley, A. J. Schmitt, J. D. Sethian, V. Serlin, J. A. Stamper, and C. A. Sullivan, et all, “The Nike KrF laser facility: Performance and initial target experiments” Physics of Plasmas 3, 2098–2107 (1996); https://doi.org/10.1063/1.871661

3. José Danglad-Flores, Stephan Eickelmann, Hans Riegler, “Deposition of polymer films by spin casting: A quantitative analysis,” Chemical Engineering Science, Volume 179, 2018, Pages 257-264, ISSN00092509, https://doi.org/10.1016/j.ces.2018.01.012.

4. T. Sakaiya, “Experimental investigation of ablative Rayleigh-Taylor instability,” Ph.D. thesis, Osaka University, 2005.

5. Lipson, H. (Henry). “Optical transforms,” London: Academic Press, 1972.

6. Hutley, M. C. Diffraction gratings. NY: Academic Press, 1982.

7. Sylvain Lazare, Vincent Granier; “Excimer laser light induced ablation and reactions at polymer surfaces as measured with a quartz-crystal microbalance.” *Journal of Applied Physics* 15 March 1988; 63 (6): 2110–2115. https://doi.org/10.1063/1.341091

8. Jenkins, Francis A., and Harvey E. White. “Fundamentals of Optics. New York,” McGraw-Hill Book Co., 1957.
9. Parkinson, Ronald. “Electroforming - a unique metal fabrication process.” (2000).

10. Wright, D., Greve, P., Fleischer, J. et al. “Laser beam width, divergence and beam propagation factor — an international standardization approach.” Opt Quant Electron 24, S993–S1000 (1992). https://doi.org/10.1007/BF01588600

11. B.A. See, “Measuring laser divergence, Optics & Laser Technology,” Volume 29, Issue 2,1997,Pages 109-110, ISSN 0030-3992, https://doi.org/10.1016/S0030-3992(97)00052-2.

12. G.N. Lawrence, “Talbot Imaging”, 1989

13. Paul Latimer and Randy F. Crouse, "Talbot effect reinterpreted," Appl. Opt. 31, 80-89 (1992) https://doi.org/10.1364/AO.31.000080

14. J. Joseph Armstrong, Terrance J. Kessler, “Large-aperture, high-efficiency holographic gratings for high-power laser systems,” Proc. SPIE 1870, Laser Coherence Control: Technology and Applications, (1 May 1993); doi:10.1117/12.154488

15. R. Srinivasan and Bodil Braren,” Ultraviolet laser ablation of organic polymers,” Chem. Rev. 1989, 89, 6, 1303–1316 Publication Date: September 1, 1989 https://doi.org/10.1021/cr00096a003

16. S. Lazare and V. Granier, “Ultraviolet laser ablation of polymers: Yield and spatial distribution of products deposition,” Chemical Physics Letters Volume 168, number 6 (1990) doi: 10.1016/0009-2614(90)85678-6

17. Sylvain Lazare, Vincent Granier; “Ultraviolet Laser Photoablation of Polymers: A Review and Recent Results”, Laser Chem. Vol. 10, pp. 25-40 (1989) https://doi.org/10.1155/1989/18750

18. V. Srinivasan, Mark A. Smrtic, S. V. Babu; “Excimer laser etching of polymers,” Journal of Applied Physics 1 June 1986; 59 (11): 3861–3867. https://doi.org/10.1063/1.336728

19. Karasik, Max, Weaver, J , Aglitskiy, Y , Oh, Juik , Obenschain, S. (2015). “Suppression of Laser Nonuniformity Imprinting Using a Thin High-Z Coating,” Physical Review Letters. doi: 114. 085001.10.1103/PhysRevLett.114.085001

20. Y. Aglitskiy, M. Karasik, A. L. Velikovich, V. Serlin, J. Weaver, T. J. Kessler, A. J. Schmitt, S. P. Obenschain, N. Metzler, and J. Oh, “Observation of Strong Oscillations of Areal Mass in an Unsupported Shock Wave,” Phys. Rev. Lett. 109, 085001 Published 20 August 2012; DOI:https://doi.org/10.1103/PhysRevLett.109.085001

21. Y. Aglitskiy, M. Karasik, A. L. Velikovich, V. Serlin, J. L. Weaver, T. J. Kessler, S. P. Nikitin, A. J. Schmitt, S. P. Obenschain, N. Metzler, and J. Oh, “Observed transition from Richtmyer-Meshkov jet formation through feedout oscillations to Rayleigh-Taylor instability in a laser target,” Physics of Plasmas 19, 102707 (2012); https://doi.org/10.1063/1.4764287

22. Kong, F M, Buckley, S R, Giles, Jr, C L, Haendler, B L, Hair, L M, Letts, S A, Overturf, III, G E, Price, C W, and Cook, R C. 1991. "Low-density carbonized resorcinol-formaldehyde foams. Final report". United States. https://doi.org/10.2172/6108157. https://www.osti.gov/servlets/purl/6108157.

23. E. C. Harding, R. P. Drake, Y. Aglitskiy, T. Plewa, A. L. Velikovich, R. S. Gillespie, J. L. Weaver, A. Visco, M. J. Grosskopf, J. R. Ditmar; “Laser driven supersonic flow over a compressible foam surface on the Nike laser,” Physics of Plasmas 1, May 2010; https://doi.org/10.1063/1.3314335

24. T-C. Chang, P.A. Molian, “Excimer pulsed laser ablation of polymers in air and liquids for micromachining applications,” Journal of Manufacturing Systems, Volume 18, Issue 2, Supplement 1,1999,Pages 1-17,ISSN 0278-6125, https://doi.org/10.1016/S0278-6125(99)80022-3.

25. T. Watari, M. Nakai, H. Azechi, T. Sakaiya, H. Shiraga, K. Shigemori, S. Fujioka, K. Otani, K. Nagai, A. Sunahara, H. Nagatomo, and K. Mima, “Rayleigh–Taylor instability growth on low-density foam targets”, Physics of Plasmas 15, 092109 (2008); https://doi.org/10.1063/1.2980419

ACKNOWLEDGEMENTS

The authors would like to thank Erik Harding and the University of Michigan for providing carbonized RF targets and quantifying the laser machined surface perturbations. Thank the Laser Plasma Branch in the Plasma Physics Division for lending their expertise in excimer lasers and use of a variety of specialized equipment. Thanks our colleagues at Optical and Imaging Sciences Group at the Laboratory for Laser Energetics for allowing observation and explanation of their diffraction grating manufacturing setup including homogenizing optical systems.